The current issue and full text archive of this journal is available at
www.emeraldinsight.com/0961-5539.htm

Numerical issues in modelling macrosegregation during DC casting of a multi-component aluminium alloy

Q. Du and D.G. Eskin
Netherlands Institute for Metals Research, Delft, The Netherlands, and
L. Katgerman
Delft University of Technology, Delft, The Netherlands

Received November 2007
Revised December 2007
Accepted 12 May 2008

Abstract

Purpose – The purpose of this paper is to investigate the ways to diminish or eliminate numerical diffusion and dispersion. Numerical dispersion and diffusion are present in the predicted macrosegregation profiles reported in the literature and they hinder the interpretation of the simulation results. With the motivation to eliminate these numerical problems by employing appropriate meshes, simulations of macrosegregation in a billet direct-chill cast from a multi-component aluminium alloy has been performed.

Design/methodology/approach – First the idea that numerical dispersion could be alleviated by refining the structured mesh size is tested and the extent of this mesh refining to overcome these numerical problems is discussed. Second the link of numerical dispersion and diffusion to the type of mesh used is investigated.

Findings – Unstructured mesh eliminates the numerical dispersion present in the structured mesh while it introduces the numerical diffusion. It is concluded by performing calculations with the same settings but different meshes that, although refining the structured mesh could alleviate the numerical oscillation, it increases the computation time dramatically. Therefore the best solution to overcome these numerical problems is the employment of a hybrid mesh consisting of both structured and unstructured mesh.

Originality/value – This work reveals the reasons behind the numerical dispersion and diffusion in macrosegregation modelling and gives a practical solution.

Keywords Modelling, Dispersions, Meshes, Alloys, Diffusion

Paper type Research paper

Nomenclature

c_p	Specific heat (J/kg K)	p	Pressure (N/m^2)
C	Mass fraction of alloy element	L	Latent heat (J/kg)
D	Mass diffusion coefficient (m^2/s)	m_s	Liquidus slope (K)
f	Mass fraction	R_E	Eutectic reaction rate (K^{-1})
g	Volume fraction	t	Time (s)
H	Enthalpy (J/kg)	T	Temperature (K)
k	Equilibrium partition coefficient	T_{Eut}	Eutectic reaction temperature (K)
K	Permeability (m^2)	T_{Liq}	Liquidus with composition C_m (K)

The authors would like to thank Dr Ian Hamill and Paul Guilbert for providing a customized version of CFX 5.7.1. This work is performed within the framework of the research program of the Netherlands Institute for Metals Research (www.nimr.nl), Project MC4.02134.

International Journal of Numerical Methods for Heat & Fluid Flow
Vol. 19 No. 8, 2009
pp. 917-930

0961-5539
DOI 10.1108/09615530910994423

T_{Sol}	Solidus with composition C_m (K)	μ	Dynamic viscosity (kg/s m)
V	Velocity (m/s)	ρ	Density (kg/m^3)
β_C	Solutal expansion coefficient	Subscripts *l, s* and *m* denote liquid, solid and mixture, respectively. Superscript *i* denotes alloying element *i*.	
β_T	Thermal expansion coefficient (1/K)		
λ	Thermal conductivity (W/m K)		

Introduction

Macrosegregation modelling has become a working instrument, which not only attracts the research interests of metallurgist, but also researchers from mechanical engineering (Han *et al.*, 2007); however when it comes to modelling DC casting, numerical dispersion and diffusion are present in the predicted macrosegregation profiles reported in literature. For example the predicted radial macrosegregation profile by Reddy and Beckermann (1997) shows the numerical dispersion. The reasons for this oscillation may be the size of the rectangular mesh used, which is about 4 mm and too coarse. In Vreeman *et al.* (2000), the sharp variation in copper composition close to the billet surface appeared and the authors attributed it to the existence of large solid fraction gradients and the inability to adequately resolve the flow field just above and below the liquidus surface highlighting the importance of mesh size. A kind of hybrid rectangular mesh in terms of mesh size is used by Thevik *et al.* (1999). In the horizontal direction it is refined when it comes closer to the surface where large concentration gradient is present. The maximum mesh size is at the billet center and is about 1 cm. The minimum one is at the surface and is about 1 mm. The mesh size is also refined in the sump region along the casting direction and its size is about 0.5 mm. However due to the structured nature of this mesh, the refinement in the sump cannot be achieved at the center and a very high aspect ratio defined by $\frac{\Delta x}{\Delta y}$ is present there, which could hinder the solution of macroscopic equations if thermo-solutal convection is present.

Some research works were dedicated to understanding and eliminating these numerical problems (Venneker and Katgerman, 2000, 2002). In Venneker and Katgerman (2000), the numerical diffusion introduced by discretization schemes was discussed and it was concluded that the numerical diffusion could be avoided by aligning the mesh with the flow field, again indicating the importance of the mesh. The authors attributed the numerical dispersion to the insufficient resolution of the permeability, i.e. the insufficient resolution of the solid fraction field. Venneker and Katgerman (2002) also tested different numerical schemes and concluded that numerical predictions can be improved not only by decreasing the computational cell size, but also with the correct choice of discretization scheme.

We can conclude that if the mesh used is not fine enough, which is a general case upon modelling big real-scale problems due to the limitation of the computing power, numerical dispersion could occur. Although numerical dispersion could be avoided by employing so called "stabilized numerical technique" such as upwind scheme, numerical diffusion could occur instead of numerical dispersion, which is also detrimental for the results and only can be alleviated by fine mesh.

Motivated by these observations, we think it is worth to investigate the ways to diminish or eliminate numerical diffusion and dispersion as the availability of parallel computing technique and sophisticated simulation software allows exploring this problem in a rigorous way, which may have been prohibitive previously.

The first question to be addressed is: at what extent of structured mesh refining the numerical dispersion can be eliminated or the simulation results can be considered as reliable. It is generally accepted that these numerical problems can be minimized by refining structured mesh although investigations about the criterion of being a "good" mesh are rare in the literature. As it is concluded in our recent publication (Eskin *et al.*, 2006) by employing an analytical method, the extent of shrinkage-induced macrosegregation is associated with the slope of the coherency fraction contour. It indicates that the macrosegregation profile is related to the secondary derivative of the coherency contour. The coherency fraction contour has to be "second derivative smooth" in order to have a good prediction of the segregation profile highlighting the importance of the spatial resolution of the temperature, or enthalpy, field. Another reason why the thermal boundary layer has to be resolved is that permeability is very sensitive to the variation of the solid fraction, which is essential associated with temperature, and bad resolution of solid fraction leads to a big variation of the permeability, thus affecting velocity field. With these in mind, it is expected that a criterion of a "good" mesh size could be proposed by analysing the temperature field and its gradient.

The second question we want to answer is: will the unstructured mesh help in eliminating the numerical dispersion and diffusion? Venneker (2003) recommended unstructured mesh for future study in order to overcome the two drawbacks of the use of structured mesh, namely the non-alignment of the mesh and the flow field, and the inability to increase the mesh density only in regions where it is necessary. In our paper the advantages associated with the use of unstructured mesh will be investigated.

The third issue we want to address is the use of hybrid mesh consisting of structured and unstructured mesh. The reason why the hybrid mesh is employed is mainly the compromise of the computation time and computational accuracy. To decrease computation time it is not optimal to use very fine mesh in the whole calculation domain such as in the solid zone where almost no solute transfer occurs owning to a negligible diffusion coefficient. Unstructured meshes can be adopted and this would reduce the total mesh number, and then, the computation time. However, as Du *et al.* (2007) demonstrate if the zone where the solid fraction is equal to 1 is meshed unstructuredly and coarsely to reduce computation time, numerical diffusion along the radius occurs even though a second order numerical scheme is used. This could be caused by the fact that this unstructured mesh does not provide the alignment of the mesh to the velocity at which the solid is moving. Hence the only solution to this dilemma is to use the hybrid meshes consisting of unstructured and structured ones. Unstructured and finer mesh in the liquid and mushy zones can guarantee a good spatial resolution and eliminate the numerical diffusion and dispersion there (Venneker, 2003), while the structured mesh created close to the surface can reduce the numerical diffusion by providing the alignment of the mesh with the flow direction. In our paper the three questions will be answered by comparing simulations results obtained with the same setting but various meshes and numerical schemes.

In the next section, a model description is presented, followed by the section of Numerical implementation. Then the calculation results are discussed, and a reliable and affordable solution to these numerical problems is given. Conclusions are given in the last section.

Model description

The macrosegregation model consists of three parts: a macroscopic transfer module, a microsegregation module and a phase diagram calculation module. The rigid network

model, originally formulated by Bennon and Incropera (1987) and re-assessed by Prescott and Incropera (1991), is adopted as the macroscopic description to predict macrosegregation during DC casting of multi-component alloys. Table I summarizes the mathematical formulation of the rigid network model.

The closure of the set of conservation equations listed in Table I requires supplementary relationships for phase mass fraction and composition, which can be derived from microscopic scale considerations. These relationships for multi-component alloys can be obtained based on the Gulliver-Scheil equation and they are listed in Table II.

Mass conservation	$\frac{\partial \rho_m}{\partial t} + \nabla \cdot (\rho_m \vec{V}_m) = 0$
Momentum conservation	$\frac{\partial (\rho_m \vec{V}_m)}{\partial t} + \nabla \cdot (\rho_m \vec{V}_m \vec{V}_m) = -\nabla p_l + \nabla \cdot (\mu_l \frac{\rho_m}{\rho_l} \nabla \vec{V}_m) - \frac{\mu_l \rho_m}{K \rho_l} (\vec{V}_m - \vec{V}_{cast}) - \rho_l (\beta_{T,l}(T - T_0) + \sum_{i=1}^{n} \beta^i_{C,l}(C^i_l - C_0))\vec{g}$, $K = K_0 \frac{(1-f_s)^3}{f_s^2}$ [16]
	n is the number of alloying elements. $\vec{V}_{cast}$ is the casting velocity. K_0 is permeability constant
Heat conservation	$\frac{\partial (\rho_m H_m)}{\partial t} + \nabla \cdot (\rho_m H_m \vec{V}_m) = \nabla \cdot (\lambda_m \nabla T) - \nabla \cdot (\rho_m (H_l - H_m)(\vec{V}_m - \vec{V}_{cast}))$
Species conservation	$\frac{\partial (\rho_m C^i_m)}{\partial t} + \nabla \cdot (\rho_m C^i_m \vec{V}_m) = \nabla \cdot (\rho_m f_l D_l \nabla C^i_m) + \nabla \cdot (\rho_m f_l D^i_l \nabla (C^i_l - C^i_m)) - \nabla \cdot (\rho_m (C^i_l - C_m)(\vec{V}_m - \vec{V}_s))$
Auxiliary relations	$\rho_m = g_s \rho_s + g_l \rho_l$ $\quad H_m = f_s H_s + f_l H_l$
	$1 = g_s + g_l$ $\quad C^i_m = f_s C^i_s + f_l C^i_l$
	$f_l = \frac{g_l \rho_l}{\rho_m}$ $\quad c_{pm} = f_s c_{ps} + f_l c_{pl}$
	$f_s = \frac{g_s \rho_s}{\rho_m}$ $\quad \lambda_m = g_s \lambda_s + g_l \lambda_l$
	$\vec{V}_m = f_s \vec{V}_s + f_l \vec{V}_l$ $\quad H_s = c_{ps} T$
	$H_l = c_{ps} T_{Sol} + c_{pl}(T - T_{Pure}) + L$

Table I.
Main equations that comprise the macrosegregation model used in this work

Gulliver-Scheil equation
$T > T_{Liq}(C^i_m), \quad f_l = 1, \quad C^i_l = C^i_m$
$T_{Liq} \geq T > T_{Eut}, \begin{cases} C^i_m = \int_0^{1-f_l} k^i C^i_l(f'_s) df'_s + f_l C^i_l \\ T = T_{Liq}(C^i_l) \end{cases}$
$T \leq T_{Eut}, \begin{cases} f_l = \max(f_l(T^+_{Eut}) + R_E(T - T_{Eut}), 0.0) \\ C^i_l = C^i_{Eut} \end{cases}$

Table II.
Supplementary relationships required for the closure of the macroscopic conservation equations

The microsegregation module is a stand-alone application program that is coupled with the ThermoCalc software to deal with multi-component alloys. Please refer to Du *et al.* (2007) for details of this model.

Numerical implementation

The macrosegregation model was implemented using the commercial software CFX, with the exception of the additional advection-like source term in the enthalpy and the solute transfer equation. These terms were implemented within a custom version of the CFX-5.7.1 solver. This implementation takes full advantages of the features provided by the commercial CFD software, CFX-5, such as unstructured meshing and parallel computing.

The model is applied to a round billet 200 mm in diameter and 453 mm in length. The length of hot top, mould, air gap and impingement zone are 20, 15, 10 and 8 mm, respectively. Only the bottom part of the hot top is modelled and the rest is considered to be a melt reservoir. The secondary cooling zone consists of Wall 1 and Wall 2, both of which are 200 mm in length. The settings for the billet and mould dimensions are identical to those used in experiments described elsewhere by Eskin *et al.* (2004). An axi-symmetric 2D model was used in this work. The melt of an Al-3.5 wt% Cu-1.5 wt% Mg alloy at a temperature of 997 K enters the hot top at the casting speed 120 mm/min multiplied by the ratio between the densities of the solid and liquid phases. A no-slip flow boundary condition is applied on all of the walls. To make the solid, which adheres to the walls of the mould, the air gap, impingement and water film domains, to have the velocity equal to the casting speed, the velocities of the walls of all mentioned domains are set to be equal to the casting speed. The boundary condition for the heat transfer equation is that, at the inlet, the melt enters at the casting temperature and, at the outlet, adiabatic boundary condition is applied. The hot top does not extract any heat but the chill mould, impingement zone, air gap and water film zones do. The heat fluxes on these walls are calculated by heat transfer coefficients, which are 5,000, 10,000, 2,500 and 10,000 $W/m^2/K$, respectively (Venneker, 2003). These boundary conditions together with the mesh used are shown in Figure 1.

Other input parameters required for this model are related to thermodynamic and physical properties of the chosen alloy and are listed in Table III (Du *et al.*, 2006; Brandes and Brook, 1992, Vol 1966). For the sake of simplicity, the diffusion coefficients of the species are taken equal to each other. Calculations were performed for steady-state conditions that have been reached in the reference experiments (Nadella *et al.*, 2006).

All of the performed calculations have taken into account solidification shrinkage and thermo-solutal buoyancy. The Gulliver-Scheil equation coupled with ternary phase diagram is employed to model the microscopic solidification behaviour. The simulation is performed with structured, unstructured or hybrid meshes, all of which can be created at various mesh sizes.

The main characteristics of calculations performed are illustrated in Table IV. The various meshes used are shown in Figure 2.

Please note that for a structured mesh, the size given in Table IV is the width/height of the rectangle mesh. For unstructured mesh, it is the edge length. The reason why only the part at the outer radius is meshed with structured mesh is that high concentration gradient present there may enforce the numerical diffusion. It will be discussed in results and discussion section.

To compare the computation speed CPU times for each second of simulation time is used as indicators and they are given in Table IV.

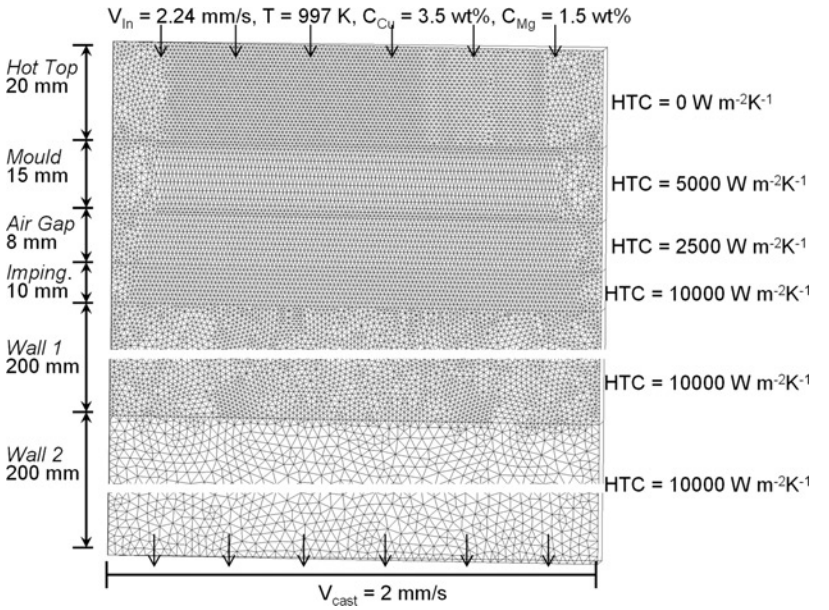

Figure 1.
The geometry of the calculation domain and the boundary conditions imposed

Prop.	Values	Prop.	Values	Prop.	Values
μ_l	0.0013 kg m^{-1}/s	D_l^{Mg}	3×10^{-9} m^2/s	c_s	958 J/kg/K
ρ_l	2460 kg/m^3	c_l	1054 J/kg/K	λ_s	180 W/m/K
$\beta_{T,l}$	1.17×10^{-4} K^{-1}	λ_l	95 W/m/K	K_0	6.67×10^{-11} m^2
$\beta_{Cu,l}$	0.73	ρ_s	2750 kg/m^3	L	3.9×10^5 J/kg
$\beta_{Mg,l}$	−0.41	D_s^{Cu}	3×10^{-13} m^2/s		
D_l^{Cu}	3×10^{-9} m^2/s	D_s^{Mg}	3×10^{-13} m^2/s		

Sources: Du *et al.* (2006); Brandes and Brook (1992); Vol (1966)

Table III.
Thermodynamic and physical properties of an Al-3.5 wt% Cu-1.5 wt% Mg alloy

Results and discussion

Although all of the calculations were performed for a ternary alloy, the calculation results shown below are only for the Cu and the significance of the other alloy element, Mg, on the overall segregation pattern has been discussed elsewhere by Du *et al.* (2007).

As shown in Figure 3a, numerical dispersion is present in Cal. 1 and Cal. 1A, all of which use the structured mesh. As compared with Cal. 1, the oscillation amplitude is reduced in Cal. 1A, whose mesh is finer than the one of Cal. 1.

The idea that mesh refining could alleviate the numerical oscillation was confirmed although at the cost of quite long computation time. It is not surprising to have these oscillations and this alleviation because central differencing scheme is used to deal with the drifting term in solute transport equations, but still interesting is to answer the question what is the criterion to be a good mesh.

As discussed in the Introduction section, we need to achieve a good resolution of thermal field; otherwise an unrealistic shape of the coherence contour may be

Cal. 1	Fully structured meshes. Hot top, mould, air gap, impingement zone: 1 mm. Wall 1, stretched mesh from 1.0 to 1.5 mm. Wall 2: uniform mesh, 1.5 mm. Radial direction: stretched mesh. Centerline: 1.5 mm; at outer radius: 0.5 mm. The total number of elements is approximately 38,000 hex elements, high resolution schemes for advection terms The CPU time for 1 s simulation time is 1,300 s
Cal. 1A	The same as Cal. 1 but with refined mesh. Hot top, mould, air gap, impingement zone: 0.5 mm. Wall 1, stretched mesh from 0.5 to 0.75 mm. Wall 2: uniform mesh, 0.75 mm. Radial direction: stretched mesh. Centerline: 0.75 mm; at outer radius: 0.25 mm. The total number of elements is approximately 154,614 hex elements, the CPU time for 1 s simulation time is 4,000 s
Cal. 2	Medium fully unstructured meshes. Hot top, mould, air gap, impingement zone: 1 mm. Wall 1 and Wall 2: 2 mm. The total number of elements is 71,784 triangles, high resolution schemes for advection terms The CPU time for 1 s simulation time is 1,025 s
Cal. 3	Coarse hybrid meshes. Hot top, mould, air gap, impingement zone and Wall 1: 1.5 mm. Wall 2: 3 mm. 30 layers of structured meshes with first prism height 0.75 mm at the outer radius and expanding to the centerby a factor 1.05. Elements consist of 5,325 quads, and 19,859 triangles, high resolution schemes for advection terms The CPU time for 1 s simulation time is 240 s
Cal. 4	Medium hybrid meshes. Hot top, mould, air gap, impingement zone, Wall 1: 1 mm. Wall 2: 2 mm. 30 layers of structured meshes with first prism height 0.5 mm at the outer radius and expanding to the center by a factor 1.05. Elements consist of 7,215 quads, and 41,436 triangles, high resolution schemes for advection terms The CPU time for 1 s simulation time is 575 s
Cal. 5	Fine hybrid meshes. Hot top and mould: 0.3 mm, air gap and impingement zone: 0.5 mm, Wall 1: 1 mm, Wall 2: 2 mm. 30 layers of structured meshes with first prism height 0.5 mm at the outer radius and expanding to the center by a factor 1.05. Elements consist of 7,215 quads, and 126,971 triangles, high resolution schemes for advection terms. (Its result is almost the same as 4A and not given in the paper)

Table IV.
Main characteristics of calculations performed in the present work

produced, which in turn affects the prediction of the final surface segregation profile. Considering a 1D case or the vertical direction of 2D case, a simple criterion would be that between two adjacent cells the variation of solid fraction should not exceed a critical number, $\Delta f_s^{Critical}$. Since the variation of solid fraction between two adjacent cells can be related to their temperature variation by the following equation, the criterion takes the following form:

$$\left|\frac{\Delta f}{\Delta T}\Delta T\right| \leq \Delta f_s^{Critical} \tag{1}$$

Consider a cell size denoted by Δx and use:

$$\Delta T = \frac{\Delta T}{\Delta x}\Delta x \tag{2}$$

so,

$$\left|\frac{\Delta f}{\Delta T}\frac{\Delta T}{\Delta x}\Delta x\right| \leq \Delta f_s^{Critical}$$

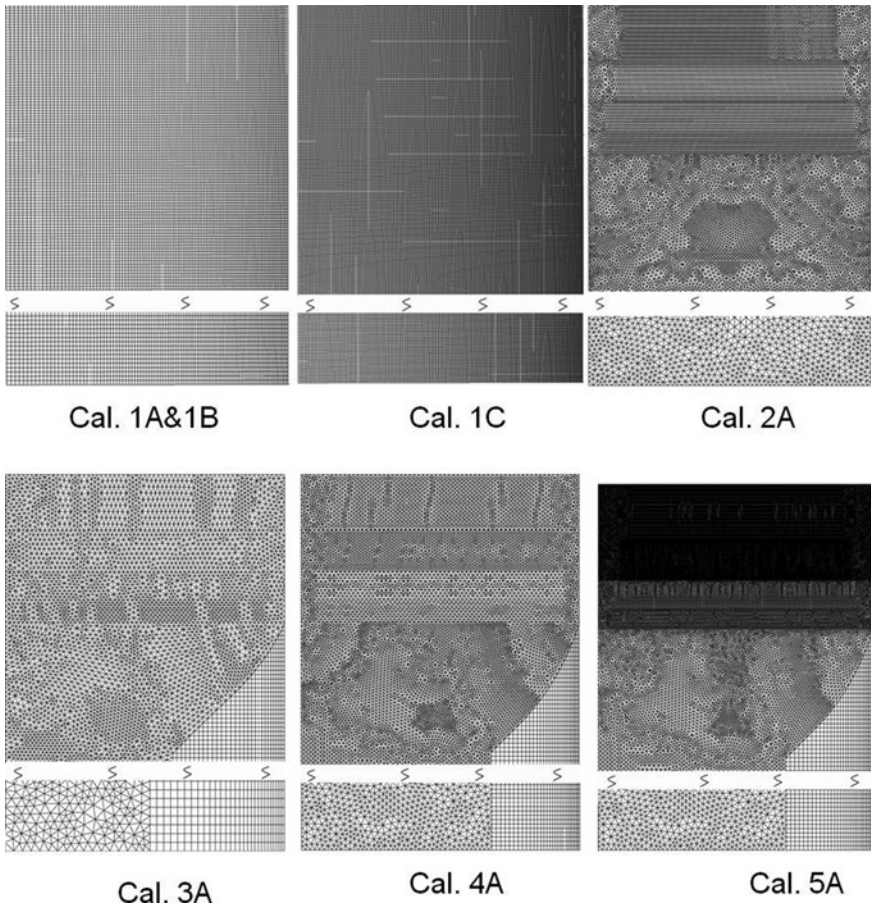

Figure 2.
Schematic for various meshes used in calculations

Arranging the above equation gives:

$$\Delta x \leq \frac{\Delta f_s^{Critical}}{\left|\frac{\Delta f}{\Delta T}\right|} \frac{1}{\left|\frac{\Delta T}{\Delta x}\right|} \tag{3}$$

For a binary alloy with linear phase diagram, assuming solidification path can be described by Scheil-Gulliver equation, we have:

$$f_s = 1 - \left(\frac{T - T_0}{mC_0}\right)^{\frac{1}{k-1}} \tag{4}$$

so,

$$\frac{df_s}{dT} = \frac{\left(\frac{T-T_0}{mC_0}\right)^{\frac{1}{k-1}}}{(1-k)(T-T_o)} = \frac{(1-f_s)^{2-k}}{(1-k)mC_0} \tag{5}$$

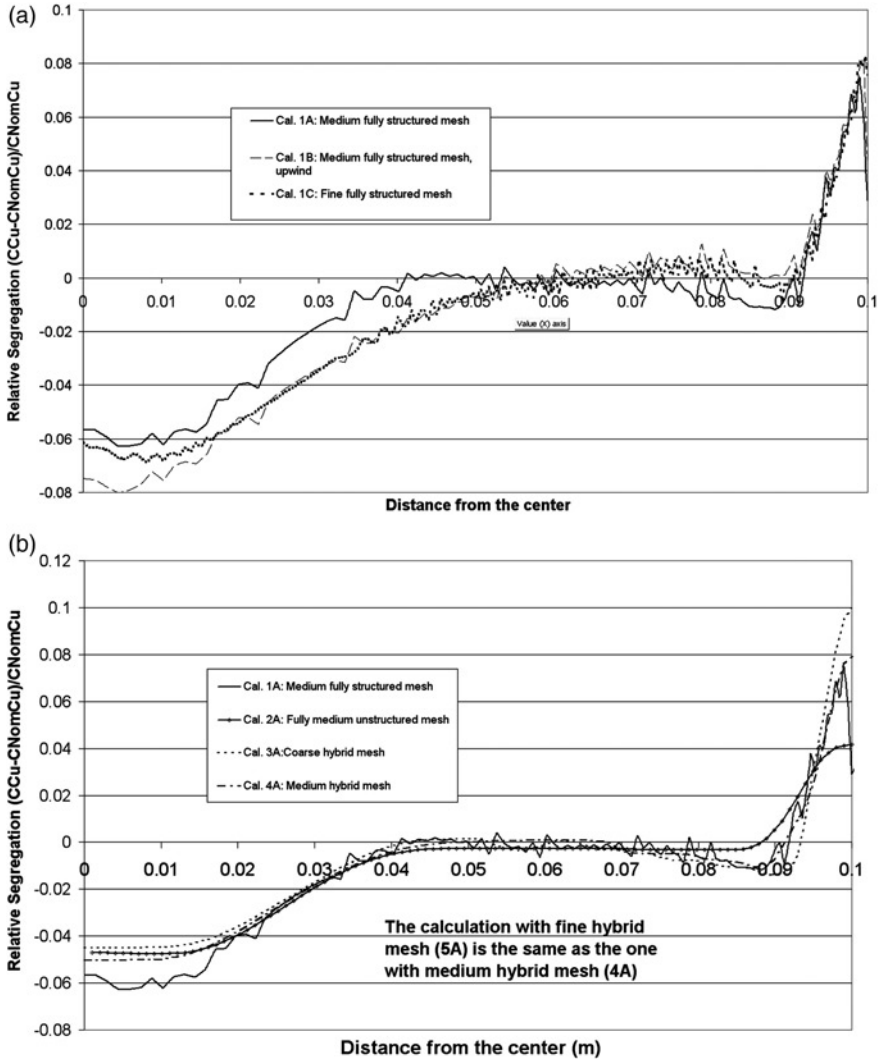

Figure 3.
The relative macrosegregation profile of Cu along the radius direction of the billet calculated with different structured mesh sizes (a) and with different types of meshes (b)

Substitute equation 5 for $\frac{\Delta f}{\Delta T}$ into equation 3 will allow one to deduce a restriction on cell size assuming the temperature gradient is known. Equation (5) reveals that $\frac{\Delta f}{\Delta T}$ decreases with increasing solid fraction. This means the restriction imposed by equation 3 would become looser as solid fraction increases.

The typical value of temperature gradient in the vicinity of the mould obtained from our calculation is 10^3K/m, although there is no an analytical expression for $\frac{\Delta f}{\Delta T}$ due to the non-linear nature of the real phase diagram, it can be easily deduced from numerically solving Scheil-Gulliver equation. We are interesting in the restriction imposed by this criterion when solid fraction is 0.05, as explained later, at which the

other criterion to be discussed later in this paper has the most severe restriction. Let us take $\Delta f_s^{Critical}$ is equal to 0.05, we have:

$$\Delta x \leq \frac{\Delta f_s^{Critical}}{\left|\frac{\Delta f}{\Delta T}\right|} \frac{1}{\left|\frac{\Delta T}{\Delta x}\right|} = \frac{0.69}{\left|\frac{\Delta T}{\Delta x}\right|} \tag{6}$$

so equation 6 will give the critical cell size of 0.69 mm. This criterion is satisfied in Cal. 1A, Cal. 4 and Cal. 5.

The other criterion is from the permeability consideration. Based on the balance between buoyancy and drag forces imposed by the dendritic matrix, Krane and Incropera (1996) deduced a relation between the appropriate velocity scale and the permeability in the mushy zone by a scaling analysis, which is given below:

$$v_0 \propto \frac{\rho g(\beta_s \Delta C_{l,0}^{\alpha} - \beta_T \Delta T_0)K}{\mu} \tag{7}$$

This relation is suitable for estimating the velocity variations in the mushy zone under the condition that porous flow dominates over viscous flow.

Consider a cell size denoted by Δx, between two adjacent cells, then one can link the velocity variations to the permeability variations induced by temperature change as:

$$\frac{\Delta v_0}{v_0} \propto \frac{\Delta K}{K} = \frac{\frac{\Delta K}{\Delta T}}{K} \Delta T = \frac{\frac{\Delta K}{\Delta T}}{K} \frac{\Delta T}{\Delta x} \Delta x \tag{8}$$

It is desirable to have this relative variation less than a critical relative velocity denoted by $\Delta v_{\mathrm{Re}l}^{Critical}$, so:

$$\Delta x \leq \frac{\Delta v_{\mathrm{Re}l}^{Critical} K}{\left|\frac{\Delta K}{\Delta T}\right|} \frac{1}{\left|\frac{\Delta T}{\Delta x}\right|} \tag{9}$$

Equation (9) is a criterion being a "good" mesh deduced from the permeability consideration.

To evaluate equation 9, the permeability and solid fraction as a function of temperature are necessary. The most widely used relation and also adopted in our calculations is Kozeny-Carmon relation, which is:

$$K = K_0 \frac{(1 - f_s)^3}{f_s^2} \tag{10}$$

Please note that for simplicity it is assumed that solid and liquid densities are equal, therefore solid mass fraction and solid volume fraction are equal.

So the derivative of permeability over solid fraction is:

$$\frac{dK}{df_s} = -K_0 \frac{2 - 3f_s + f_s^3}{f_s^3} \tag{11}$$

Assuming solidification proceeds in Scheil-type way, and for a binary alloy with linear phase diagram, combining with equation 5:

$$\frac{dK}{dT} = \frac{dK}{df_s}\frac{df_s}{dT} = K_0 \frac{(1-f_s)^2(2+f_s)\left(\frac{T-T_0}{mC_0}\right)^{\frac{1}{k-1}}}{f_s^3(k-1)(T-T_o)} \tag{12}$$
$$= K_0 \frac{(1-f_s)^3(2+f_s)}{f_s^3(k-1)(T-T_o)} = K_0 \frac{(1-f_s)^{4-k}(2+f_s)}{f_s^3(k-1)mC_0}$$

so,

$$\frac{K}{\frac{dK}{dT}} = \frac{(1-f_s)^{k-1} f_s(k-1)mC_0}{(2+f_s)} \tag{13}$$

Combining equation 13 with equation 9, we have:

$$\Delta x \leq \Delta v_{\mathrm{Re}\,l}^{Critical} \left| \frac{(1-f_s)^{k-1} f_s(k-1)mC_0}{(2+f_s)} \frac{1}{\Delta T/\Delta x} \right| \tag{14}$$

Applying equation 14 to the binary Al-4.5wt% Cu with a linear phase diagram (k = 0.171, $m_s = -340$ K), which can be regarded as a close analogy of the ternary alloy we modeled, it is readily to have a relation between $K/(\Delta K/\Delta T)$ and solid fraction as shown in Figure 4.

Although the term $K/(\Delta K/\Delta T)$ is very small when solid fraction is less 5 per cent, which would give a very tight restriction on mesh size, equation 7, which this criterion is built on, is not applicable in this rang of solid fraction because this Darcy term is not significant as a result of high permeability as discussed by Krane and Incropera (1996). The starting point where the Darcy term starts to dominate is when solid fraction is approximately 0.05, and it is where the most severe restriction is imposed over Δx. So

$$\Delta x \leq \Delta v_{\mathrm{Re}\,l}^{Critical} \frac{0.32}{\frac{\Delta T}{\Delta x}} \tag{15}$$

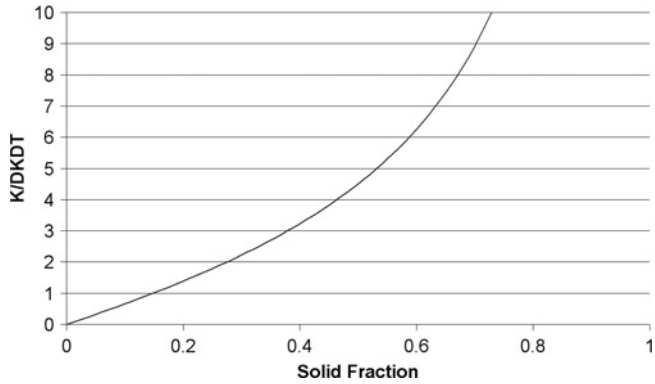

Figure 4.
$K/\frac{\Delta K}{\Delta T}$ as a function of solid fraction

Let us take $\Delta v_{\mathrm{Re}\,l}^{Critical}$ as 0.5 and equation 15 becomes

$$\Delta x \leq \frac{0.16}{\frac{\Delta T}{\Delta x}} \tag{16}$$

Compared with the equation 6, this criterion gives tighter restriction.

In our calculations, the temperature gradient in vertical direction can be as high as 1,000 K/m, and equation 16 means any mesh with size above 0.16 mm would be bad in the region around solid fraction contour of 0.05. This tight criterion is hardly to be met in the calculations; therefore it is unavoidable to have some numerical problems in calculating velocity fields around the liquidus contour.

To summarize being a "good" mesh have to satisfy the two criterions deduced above, which are put into Table V.

Another interesting comparison is between the relative segregation profiles along the radius direction of Cal. 1 on one side, and Cal. 2, 3 and 4 on the other side as shown in Figure 3b. Only Cal. 1 exhibits the numerical dispersion. The reason why numerical dispersion disappear in Cal. 2 could be that numerical diffusion present in Cal. 2 removed numerical dispersion. Numerical diffusion is present in Cal. 2 is proved by examining Figure 5, which shows the relative segregation profile along the casting direction at the surface.

In Figure 5, the X axis is the distance along the casting direction just below the inlet surface. In all of the calculations, the relative segregation is zero at the inlet surface, i.e. the relative distance of zero, where solidification still does not start and only the liquid phase is present. As the position lowered it enters the mushy zone and the relative segregation is first sharply down due to the convection bringing the solute away from

Criterions deduced based on	Maximum mesh size
Thermal filed	$\frac{\Delta f_s^{Critical}}{\left\lvert\frac{\Delta f}{\Delta T}\right\rvert}\frac{1}{\left\lvert\frac{\Delta T}{\Delta x}\right\rvert}$
Permeability filed	$\Delta v_{\mathrm{Re}\,l}^{Critical}\left\lvert\frac{(1-f_s)^{k-1}f_s(k-1)mC_0}{(2+f_s)}\frac{1}{\frac{\Delta T}{\Delta x}}\right\rvert$

Table V.
Two criterions for eliminating numerical dispersion

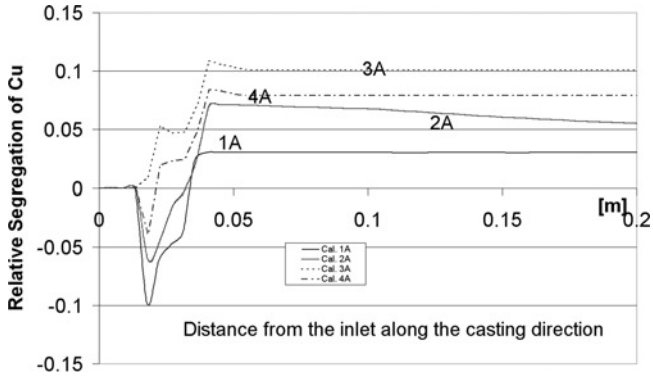

Figure 5.
The relative segregation profile along the casting direction at the surface

the surface to the centerand, then is sharply up due to the shrinkage induced flow sucking back some solute. The peak value in these curves corresponds to the position where solidification ends. Lower than this position there should not be any change in the relative segregation because the solid diffusion coefficient of the solute is negligible. However in Cal. 2 it keeps decreasing due to the numerical diffusion.

This comparison revealed that although unstructured mesh could decrease computation time by "fine meshing only the necessary region", it introduced the numerical diffusion. This numerical diffusion by no means only exists in the solid zone; it must spread the entire calculation domain. Therefore, the answer to our second questions raised in Introduction section, is that the use of unstructured mesh is two-fold. On one side, it can decrease the computation time due to the decrease in mesh number by "fine meshing only the necessary region" without sacrificing the computation speed, or, we can say it can improve the calculation accuracy without dramatically increasing the computation time if only the "necessary" region is meshed very finely. On the other side, it may introduce the numerical diffusion. Therefore it is not wise to employ unstructured mesh in the zone such as the surface of the solid zone where the flow direction is known to be straightly downwards and concentration gradients are high. Naturally the hybrid mesh is an optimal option, which leads us to the discussion on the answer to our third question raised in Introduction section.

The advantage of hybrid mesh is also shown in Figure 5. For the relative segregation profile along the casting direction at the surface, Cal. 2 suffered numerical diffusion. While in the calculation with the hybrid meshes Cal. 3 and Cal. 4, it is almost constant, and only a slightly decrease is present in a small zone in Cal. 3 and Cal. 4 after solidification is finished, which actually corresponds to the transition zone from the unstructured mesh to the structured mesh. The elimination of numerical diffusion in Cal. 3 and Cal. 4 leads to a higher average concentration than the calculation with fully unstructured mesh, Cal. 2 as shown in Figure 3b.

The advantage of hybrid mesh can be seen by the comparison of Cal. 4 with Cal. 1 and Cal. 2. As discussed above, Cal. 1 experiences numerical dispersion and Cal. 2 suffers numerical diffusion. While in Cal. 4 both of these two numerical problems have been minimized. It should be noted that the profiles calculated Cal. 4 and Cal. 5 (with finer hybrid meshes and not shown in this paper) are almost identical.

Conclusions

By performing calculations with the same settings but different meshes it is concluded that although refining the structured mesh could alleviate the numerical dispersion, it increases dramatically the computation time since the mesh has to be refined to the extent imposed by the two tight criterions. The use of fully unstructured mesh could decrease the computation time by only fine meshing the necessary region, but it may suffer numerical diffusion. Therefore the best solution to overcome these numerical problems is the employment of a hybrid mesh consisting of structured and unstructured mesh. This suggestion is confirmed by the calculations carried out in this paper.

References

Bennon, W.D. and Incropera, F.P. (1987), "A continuum model for momentum, heat and species transport in binary solid-liquid phase change systems 1: model formulation", *International Journal of Heat and Mass Transfer*, Vol. 30, pp. 2161-70.

Brandes, E.A. and Brook, G.B. (1992), *Smithells Metals Reference Book*, 7th ed., Butterworth-Heinemann, Oxford.

Du, Q., Eskin, D.G. and Katgerman, L. (2006), "Modelling macrosegregation during DC casting of a binary aluminium alloy", *Modelling of Casting, Welding and Advanced Solidification Processes XI*, TMS, France.

Du, Q., Eskin, D.G. and Katgerman, L. (2007), "Modeling macrosegregation during direct-chill casting of multicomponent aluminum alloys", *Metallurgical and Materials Transactions A*, Vol. 38A, pp. 180-9.

Eskin, D.G., Du, Q. and Katgerman, L. (2006), "Relationship between shrinkage-induced macrosegregation and the sump profile upon direct-chill casting", *Scripta Materialia*, Vol. 55, pp. 715-8.

Eskin, D.G., Zuidema, J., Savran, V.I. and Katgerman, L. (2004), "Structure formation and macro segregation under different process conditions during DC casting", *Materials Science and Engineering A*, Vol. 384, pp. 232-44.

Han, Z.Q., Lewis, R.W. and Liu, B.C. (2007), "Modelling of the thermosolutal convection and macrosegregation in the solidification of an Fe-C binary alloy", *International Journal of Numerical Methods for Heat and Fluid Flow*, Vol. 17 No. 3, pp. 313-21.

Krane, M.J.M. and Incropera, F.P. (1996), "A scaling analysis of the unidirectional solidification of a binary alloy", *International Journal of Heat and Mass Transfer*, Vol. 39 No. 17, pp. 3567-79.

Nadella, R., Eskin, D.G. and Katgerman, L. (2006), "Role of grain refining in macrosegregation upon direct chill casting of AA 2024 round billet", *Materials Science Forum*, Vol. 519-521, pp. 1891-6.

Prescott, P.J. and Incropera, F.P. (1991), "Modelling of dendritic solidification systems – reassessment of the continuum momentum equation", *International Journal of Heat and Mass Transfer*, Vol. 34 No. 9, pp. 2351-9.

Reddy, A.V. and Beckermann, C. (1997), "Modeling of macrosegregation due to thermosolutal convection and contraction-driven flow in direct chill continuous casting of an Al-Cu round ingot", *Metallurgical Materials Transactions B*, Vol. 28B No. 3, pp. 479-89.

Thevik, H.J., Mo, A. and Rusten, T. (1999), "A mathematical model for surface segregation in aluminum direct chill casting", *Metallurgical Materials Transactions B*, Vol. 30B, pp. 135-42.

Venneker, B.C.H. (2003), "Simulation of macrosegregation during direct chill casting", NIMR Publication p.03.4.006, The Netherlands.

Venneker, B.C.H. and Katgerman, L. (2000), "Macrosegregation during DC casting of aluminium alloys: numerical issues and the effect of metal entry", in Sahm, P.R. Hansen, P.N. and Conley, J.G. (Eds), *Modeling of Casting, Welding and Advanced Solidification Processes IX*, Shaker, Aachen, pp. 680-6.

Venneker, B.C.H. and Katgerman, L. (2002), "Modelling issues in macrosegregation predictions in direct chill castings", *Journal of Light Metals*, Vol. 2, pp. 149-59.

Vol, A.E. (1966), *Handbook of Binary Metallic Systems: Structure and Properties*, Vol. 1, Israel Program for Scientific Translations, Jerusalem.

Vreeman, C.J., Krane, M.J.M. and Incropera, F.P. (2000), "The effect of free-floating dendrites and convection on macrosegregation in direct chill cast aluminum alloys part I: model development", *International Journal of Heat and Mass Transfer*, Vol. 43 No. 5, pp. 687-704.

Corresponding author
Qiang Du can be contacted at: qiang.du@ubc.ca